Supporting Information

Abrams et al. 10.1073/pnas.1302982110

SI Results

Given the finding of strong autism spectrum disorder (ASD) underconnectivity between left-hemisphere posterior superior temporal sulcus (pSTS) and the distributed reward circuit (Fig. 2), we sought to examine whether abnormal connectivity of reward circuitry extended beyond those involved in processing of the human voice (1). To address this, we examined group differences in resting-state connectivity of the left-hemisphere nucleus accumbens (NAc), a key region within the reward pathway highlighted in our main results (Fig. 2). To avoid circularity, we identified the left-hemisphere NAc as defined by the Harvard–Oxford probabilistic structural atlas (2) using a probability threshold of 25%. Results from this analysis revealed ASD underconnectivity between left-hemisphere NAc and several brain structures, including bilateral pSTS and left-hemisphere mid-middle temporal gyrus of temporal cortex, bilateral medial and lateral occipital cortex, bilateral precuneus, right-hemisphere supramarginal gyrus, left-hemisphere central operculum of parietal cortex, precentral gyrus, and posterior cingulate cortex (Fig. S8). Only the anterior medial cerebellum showed ASD overconnectivity for the NAc seed (Fig. S8, *Lower*). A striking result of this analysis is the overlap between underconnected regions of bilateral pSTS identified in the NAc connectivity analysis and the pSTS seeds used in the original analysis. It is also worth noting that ASD underconnectivity of left-hemisphere NAc was not evident in any region of prefrontal cortex despite its many connections with this area of cortex (3). Taken together, the results provide evidence that, in addition to weak brain connectivity between the reward pathway and voice-selective auditory cortex, children with ASD also have aberrant connectivity between reward circuitry and brain regions involved in other sensory modalities. Additional research is needed to reconcile these findings with NAc hyperconnectivity reported in a previous study of children with ASD (4).

SI Materials and Methods

Data Acquisition. ***Functional MRI.*** Functional images were acquired on a 3-T Signa scanner (General Electric) by using a custom-built head coil. Participants were instructed to stay as still as possible during scanning, and head movement was further minimized by placing memory-foam pillows around the participant's head. A total of 29 axial slices (4.0-mm thickness, 0.5-mm skip) parallel to the anterior/posterior commissure line and covering the whole brain were imaged by using a T2*-weighted gradient-echo spiral in-out pulse sequence (5) with the following parameters: repetition time, 2,000 ms; echo time, 30 ms; flip angle, 80°; one interleave. The field of view was 20 cm, and the matrix size was 64 × 64, providing an in-plane spatial resolution of 3.125 mm. Reduction of blurring and signal loss arising from field inhomogeneities was accomplished by the use of an automated high-order shimming method before data acquisition.

Structural MRI. For each subject, a high-resolution T1-weighted spoiled-grass gradient-recalled inversion-recovery 3D MRI sequence was acquired to facilitate anatomical localization of functional data. The following parameters were used: inversion time, 300 ms; repetition time, 8.4 ms; echo time, 1.8 ms; flip angle, 15°; 22-cm field of view; 132 slices in coronal plane; 256 × 192 matrix; two excitations; and acquired resolution, 1.5 × 0.9 × 1.1 mm.

Functional MRI Preprocessing. A linear shim correction was applied separately for each slice during reconstruction by using a magnetic field map acquired automatically by the pulse sequence at the beginning of the scan. Functional MRI data were then analyzed by using SPM8 analysis software (www.fil.ion.ucl.ac.uk/spm). Images were realigned to correct for motion, corrected for errors in slice timing, spatially transformed to standard stereotaxic space [based on the Montreal Neurologic Institute (MNI) coordinate system], resampled every 2 mm by using sinc interpolation, and smoothed with a 6-mm full-width half-maximum Gaussian kernel to decrease spatial noise before statistical analysis. Translational movement in millimeters (x, y, z) and rotational motion in degrees (pitch, roll, yaw) was calculated based on the SPM8 parameters for motion correction of the functional images in each subject.

Region of Interest Selection. Coordinates for the pSTS regions of interest (ROIs) were chosen based on a previous study that showed cortical regions selective for vocal stimuli compared with acoustical control conditions in neurotypical adults (1). Peak coordinates described in that study for the contrast of vocal stimuli minus control sounds were transformed from Talaraich to MNI space by using the tal2mni function in Matlab (http://imaging.mrc-cbu.cam.ac.uk/downloads/MNI2tal/tal2mni.m). The coordinates for the left-hemisphere pSTS peak were [−63, −42, 9], and the coordinates for the two right-hemisphere pSTS peaks were [57, −31, 5] and [46, −46, 4]. The ROIs used in the functional connectivity analysis were 6-mm spheres centered on these three coordinates. To examine whether the size of ROIs affected between-group connectivity results, 8-mm spheres centered at left- and right-hemisphere pSTS peaks were used as seeds in supplementary analyses (Figs. S4 and S5). Coordinates for the low-level auditory cortical analyses were taken from a study showing cytoarchitectonically dissociable regions of auditory cortex (6). The Te1.0 region was defined as the core koniocortical field in this work. Coordinates for bilateral Te1.0 served as our primary auditory cortical (PAC) ROIs. ROIs were extracted by using the anatomy toolbox of SPM software, and the center of mass for the PAC ROIs was calculated in SPM. For the left-hemisphere PAC, coordinates for Te1.0 were [−48, −20, 6], and, for the right-hemisphere PAC, coordinates for Te1.0 were [50, −15, 5]. The ROIs used in the functional connectivity analysis were 6-mm spheres centered on these coordinates. We also performed a follow-up functional connectivity analysis by using the left-hemisphere NAc as the seed region (*SI Results* and Fig. S8). To avoid circularity with the pSTS seed analysis (Fig. 2), we identified the left-hemisphere NAc as defined by the Harvard–Oxford probabilistic structural atlas (2) using a probability threshold of 25%. This method is consistent with a previous study of intrinsic connectivity of the NAc (7).

Functional Connectivity Analysis. For each ROI, a resting-state time series was extracted by averaging the time series of all voxels within it. The resulting ROI time series was then used as a covariate of interest in a linear regression whole-brain analysis. A global time series, computed across all brain voxels, along with six motion parameters, were used as additional covariates to remove confounding effects of physiological noise and participant movement. Because of the unresolved controversies in the field surrounding the use of global signal regression in resting-state functional connectivity analyses (8–12), we conducted additional analyses in which we removed white matter and cerebrospinal fluid (CSF) confounds, as an alternative to global signal regression (8). We regressed the mean time series of a 2-mm ROI located in the center of the left lateral ventricle (MNI coordinates [−24 −44 8]) and left superior corona radiata (MNI coordinates [−24 −40 4]) in place of the global signal correction used in our primary analysis.

As can be seen from Figs. S6 and S7, the majority of our original results were unaltered by the removal of white matter and CSF confounds. No new ASD>typically developing (TD) effects are present after using this alternative analysis. The ASD and TD groups did not significantly differ in motion ($P > 0.7$) or have average RMS movement >0.35 mm. To demonstrate the robustness of our findings against potential movement confounds, we performed additional supplementary analyses. We computed correlations between movement parameters and brain connectivity values, and found that there was no significant correlation between mean brain connectivity values and RMS of displacement for any of the ROIs examined. Group-level connectivity maps were generated by using one-sample *t* tests of individual functional connectivity contrast images. Within-group functional connectivity maps were thresholded at $P < 0.000001$ uncorrected for height and 100 voxels for extent. Between-group functional connectivity maps were thresholded at $P < 0.01$ uncorrected for height and a voxel cluster extent of 100 (corresponding to $P < 0.01$ for height and $P < 0.01$ for extent).

Group mean connectivity between seed ROIs and brain regions identified in the whole-brain analysis were calculated to examine the basis for TD>ASD group differences (bar graphs in Figs. 1 and 2). The reason for this analysis is that group connectivity differences can result from a number of different factors. For example, both TD and ASD groups could show negative connectivity between the seed regions and their targets, and significant TD>ASD group differences could be driven by greater negative connectivity in subjects with ASD. Significant group differences were inherent to this ROI analysis as they are based on results from the whole-brain connectivity analysis (13); however, results provide important information regarding the magnitude and sign of connectivity results in both TD and ASD groups.

To calculate group mean connectivity within specific ROIs, we identified the voxel with maximum TD>ASD group difference from the pSTS functional connectivity analyses within each brain ROI as defined by the Harvard–Oxford probabilistic structural atlas (2) using a probability threshold of 25%. For identification of the ventral tegmental area of the midbrain, we used *Duvernoy's Atlas of the Brainstem* (14) and confirmed overlap of our connectivity map with several previously published ventral tegmental area coordinates (15, 16). We then extracted the β-value from individual subjects' contrast maps from the pSTS functional connectivity analyses using the coordinates for each of these ROIs. The mean and SEs were calculated for the TD and ASD groups, and independent-sample *t* tests were performed on these values.

Functional Connectivity Analysis Using Scrubbing Procedures. Recent work has shown that small group differences in subject movement can result in significant artifacts in functional connectivity results, with increased movement artificially reducing the strength of long-range brain connections (17). This finding is particularly concerning for autism research because reduced long-range brain connectivity represents a prominent neural theory of autism (18), and individuals with autism typically display greater subject movement during functional MRI (fMRI) data collection compared with control subjects (19). To ensure that our findings are not severely confounded by participant motion, we performed additional analyses in which we applied the "data scrubbing" method proposed by Power et al. (17). Volumes with frame-wise displacement greater than 0.5 mm and derivative variance greater than 0.5% of blood oxygen level-dependent signal were identified and excluded by using the parameters proposed previously (17).

1. Belin P, Zatorre RJ, Lafaille P, Ahad P, Pike B (2000) Voice-selective areas in human auditory cortex. *Nature* 403(6767):309–312.
2. Smith SM, et al. (2004) Advances in functional and structural MR image analysis and implementation as FSL. *Neuroimage* 23(suppl 1):S208–S219.
3. Haber SN, Knutson B (2010) The reward circuit: Linking primate anatomy and human imaging. *Neuropsychopharmacology* 35(1):4–26.
4. Di Martino A, et al. (2011) Aberrant striatal functional connectivity in children with autism. *Biol Psychiatry* 69:847–856.
5. Glover GH, Law CS (2001) Spiral-in/out BOLD fMRI for increased SNR and reduced susceptibility artifacts. *Magn Reson Med* 46(3):515–522.
6. Morosan P, et al. (2001) Human primary auditory cortex: Cytoarchitectonic subdivisions and mapping into a spatial reference system. *Neuroimage* 13(4):684–701.
7. Cauda F, et al. (2011) Functional connectivity and coactivation of the nucleus accumbens: A combined functional connectivity and structure-based meta-analysis. *J Cogn Neurosci* 23(10):2864–2877.
8. Fox MD, Zhang D, Snyder AZ, Raichle ME (2009) The global signal and observed anticorrelated resting state brain networks. *J Neurophysiol* 101(6):3270–3283.
9. Murphy K, Birn RM, Bandettini PA (2013) Resting-state fMRI confounds and cleanup. *Neuroimage*, 10.1016/j.neuroimage.2013.04.001.
10. Saad ZS, et al. (2012) Trouble at rest: How correlation patterns and group differences become distorted after global signal regression. *Brain Connect* 2(1):25–32.
11. Satterthwaite TD, et al. (2013) An improved framework for confound regression and filtering for control of motion artifact in the preprocessing of resting-state functional connectivity data. *Neuroimage* 64:240–256.
12. Weissenbacher A, et al. (2009) Correlations and anticorrelations in resting-state functional connectivity MRI: A quantitative comparison of preprocessing strategies. *Neuroimage* 47(4):1408–1416.
13. Vul E, Harris C, Winkielman P, Pashler H (2009) Puzzlingly high correlations in fMRI studies of emotion, personality, and social cognition. *Perspect Psychol Sci* 4:274–290.
14. Naidich TP, et al. (2009) *Duvernoy's Atlas of the Human Brain Stem and Cerebellum* (Springer, Vienna).
15. Bunzeck N, Düzel E (2006) Absolute coding of stimulus novelty in the human substantia nigra/VTA. *Neuron* 51(3):369–379.
16. Wittmann BC, et al. (2005) Reward-related FMRI activation of dopaminergic midbrain is associated with enhanced hippocampus-dependent long-term memory formation. *Neuron* 45(3):459–467.
17. Power JD, Barnes KA, Snyder AZ, Schlaggar BL, Petersen SE (2012) Spurious but systematic correlations in functional connectivity MRI networks arise from subject motion. *Neuroimage* 59(3):2142–2154.
18. Just MA, Cherkassky VL, Keller TA, Minshew NJ (2004) Cortical activation and synchronization during sentence comprehension in high-functioning autism: Evidence of underconnectivity. *Brain* 127(Pt 8):1811–1821.
19. Yerys BE, et al. (2009) The fMRI success rate of children and adolescents: Typical development, epilepsy, attention deficit/hyperactivity disorder, and autism spectrum disorders. *Hum Brain Mapp* 30(10):3426–3435.

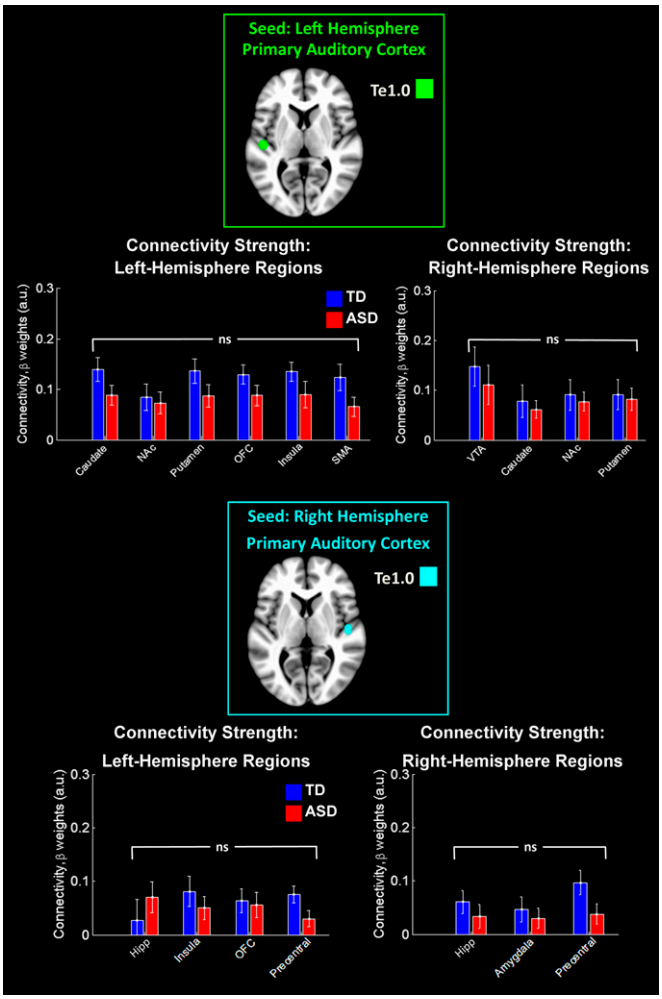

Fig. S1. Between-group functional connectivity results for bilateral PAC. (*Upper*) Left-hemisphere PAC connectivity was comparable between TD and ASD groups in brain structures that previously showed group differences in the left-hemisphere pSTS analysis (Fig. 2). Mean connectivity differences between TD children and children with ASD are plotted in the bar graphs for six left-hemisphere and four right-hemisphere regions identified in the left-hemisphere pSTS connectivity analysis (error bars represent SEM). The seed region used in this analysis was a 6-mm sphere centered in left-hemisphere PAC at MNI coordinates [−48, −20, 6] (6). Group differences for the connections displayed in the bar graphs failed to reach significance at the $P < 0.05$ level. (*Lower*) Right-hemisphere PAC connectivity was comparable between TD and ASD groups in brain structures that previously showed group differences in the right-hemisphere pSTS analysis (Fig. 3). Mean connectivity differences between TD children and children with ASD are plotted in the bar graphs for four left-hemisphere and three right-hemisphere regions identified in the right-hemisphere pSTS connectivity analysis (error bars represent SEM). The seed region used in this analysis was a 6-mm sphere centered in right-hemisphere PAC at MNI coordinates [50, −15, 5] (6). Group differences for the connections displayed in the bar graphs failed to reach significance at the $P < 0.01$ level; however, one connection was significant at the $P < 0.05$ level (left-hemisphere precentral gyrus; $P = 0.0498$). Hipp, hippocampus; OFC, orbitofrontal cortex; SMA, supplementary motor area; VTA, ventral tegmental area.

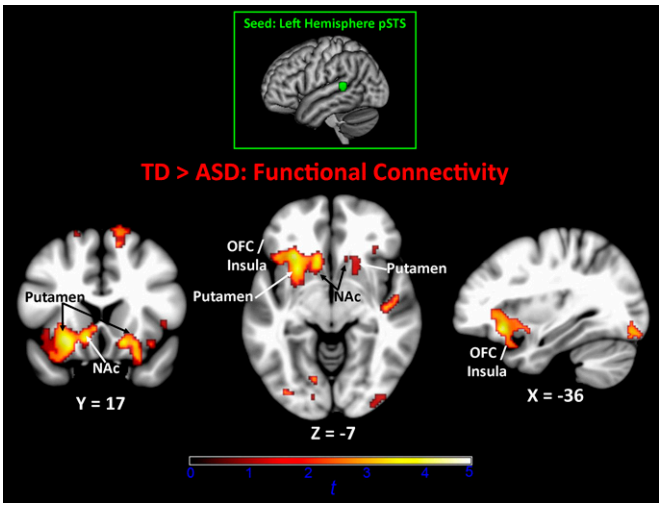

Fig. S2. Between-group functional connectivity results for left-hemisphere speech-selective cortex using scrubbed fMRI data. After controlling for participant motion using the scrubbing procedure (17), group differences for the TD>ASD contrast continued to indicate ASD underconnectivity between left-hemisphere pSTS and structures of the reward network, including the NAc, insula, and orbitofrontal cortex. The seed used in this analysis was a 6-mm sphere centered in left-hemisphere pSTS at MNI coordinates [−63, −42, 9] (1). Images are thresholded at $P < 0.01$ for voxel height and an extent of 100 voxels.

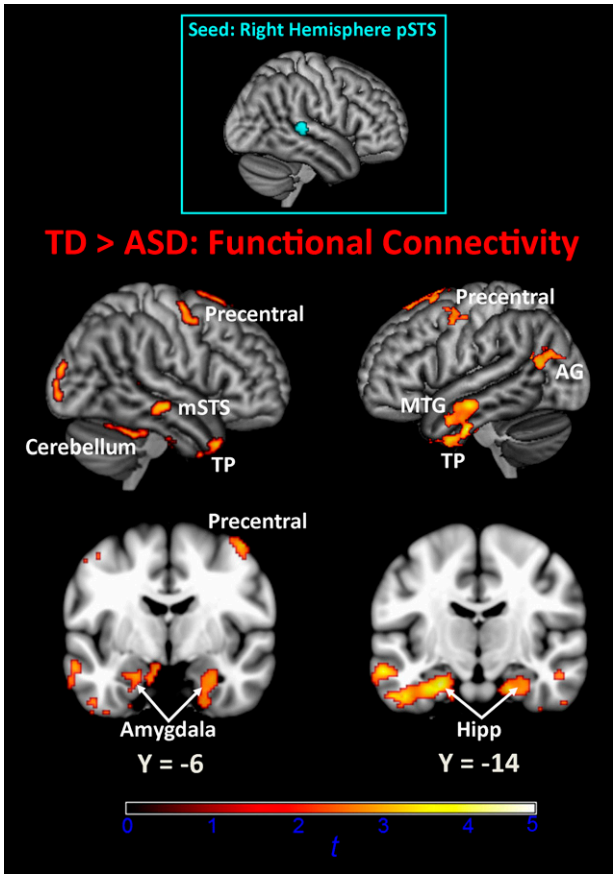

Fig. S3. Between-group functional connectivity results for right-hemisphere speech-selective cortex using scrubbed fMRI data. After controlling for participant motion using the scrubbing procedure (17), group differences for the TD>ASD contrast continued to indicate ASD underconnectivity between right-hemisphere pSTS and brain structures serving reward, emotional, memory, and motor functions. The seed region used in this analysis was a 6-mm sphere centered in right-hemisphere pSTS at MNI coordinates [57, −31, 5] (1). Images are thresholded at $P < 0.01$ for voxel height and an extent of 100 voxels. AG, angular gyrus; Hipp, hippocampus; mSTS, mid-superior temporal sulcus; MTG, middle temporal gyrus; TP, temporal pole.

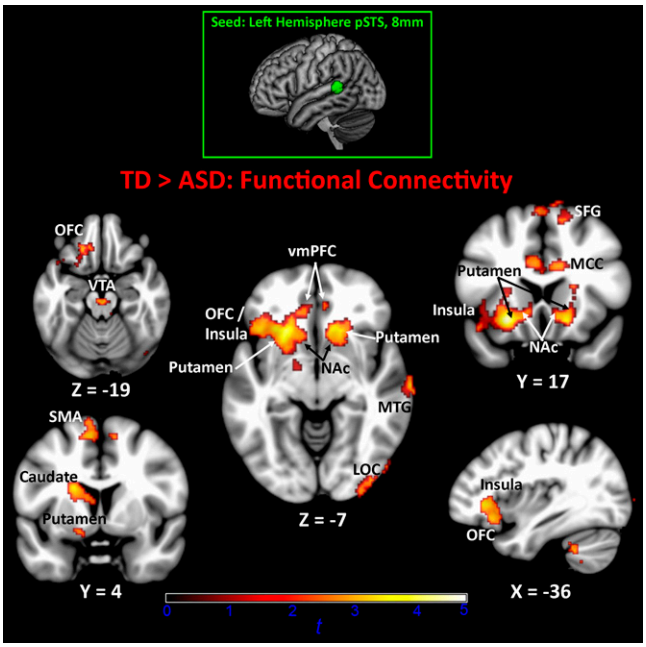

Fig. S4. Between-group functional connectivity results for left-hemisphere speech-selective cortex using an 8-mm sphere as the seed region. In our main analysis, we used a 6-mm sphere for the left-hemisphere pSTS seed to ensure anatomical specificity for voice-selective regions of cortex (1). Here, we investigated whether increasing the seed region to 8-mm spheres affected TD>ASD connectivity results. Results show nearly identical results as those shown in the main results (Fig. 2). Specifically, results show decreased connectivity of left-hemisphere pSTS in children with ASD in the distributed reward circuit, including bilateral ventral tegmental area (VTA), NAc, ventromedial prefrontal cortex (vmPFC), left-hemisphere dorsal caudate, anterior insula, and orbitofrontal cortex. ASD underconnectivity was also evident in motor planning regions including bilateral MCC and supplementary motor area, as well as right-hemisphere middle temporal gyrus (MTG), bilateral superior frontal gyrus (SFG), and lateral occipital cortex (LOC). Images are thresholded at $P < 0.01$ for voxel height and an extent of 100 voxels. MCC, mid-cingulate cortex; OFC, orbitofrontal cortex; SMA, supplementary motor area.

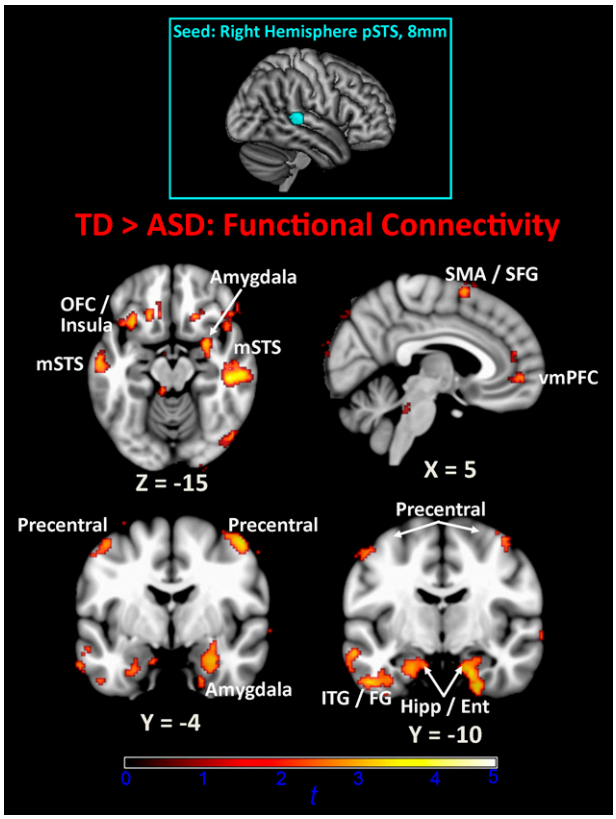

Fig. S5. Between-group functional connectivity results for right-hemisphere speech-selective cortex using an 8-mm sphere as the seed region. In the main analysis, we used a 6-mm sphere for the right-hemisphere pSTS seed to ensure anatomical specificity for voice-selective regions of cortex (1). Here, we investigated whether increasing the seed region to 8-mm spheres affected TD>ASD connectivity results. Again, results show nearly identical results as those shown in the main results (Fig. 3). Specifically, results show ASD underconnectivity of right-hemisphere amygdala and supplementary motor area as well as bilateral mid-superior temporal sulcus (mSTS), ventromedial prefrontal cortex (vmPFC), precentral gyrus, and hippocampus. Images are thresholded at $P < 0.01$ for voxel height and an extent of 100 voxels. Ent, entorhinal cortex; ITG, inferior temporal gyrus; Hipp, hippocampus; OFC, orbitofrontal cortex; SFG, superior frontal gyrus; SMA, supplementary motor area.

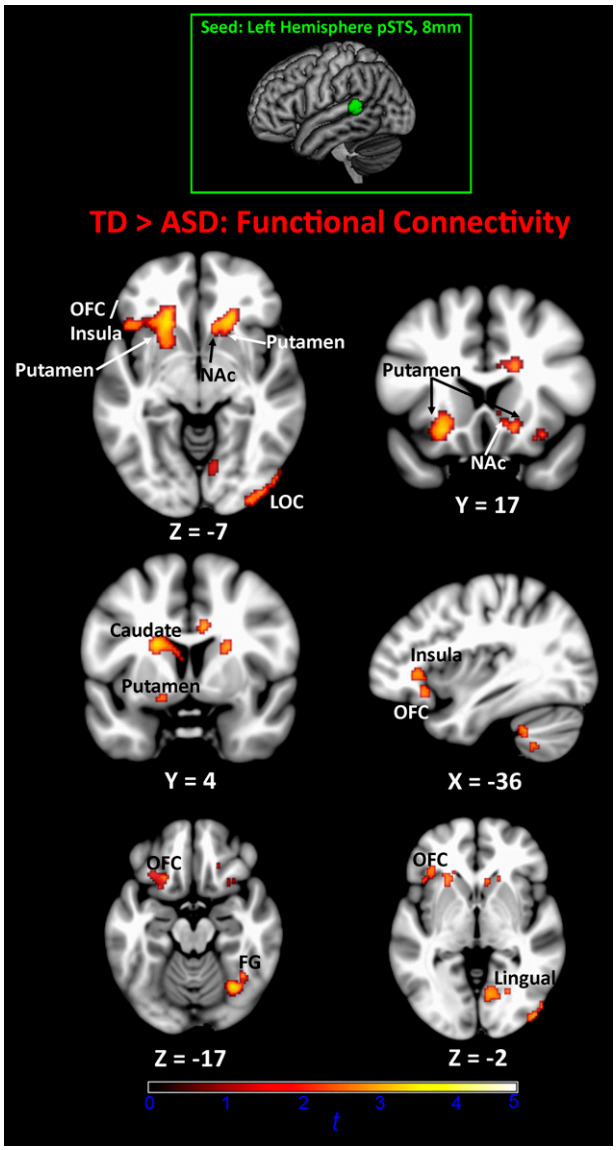

Fig. S6. Between-group functional connectivity results for left-hemisphere speech-selective cortex after removing white matter and CSF confounds. In the main analysis, we performed global signal regression, which is a common approach for resting-state functional connectivity analyses. However, there is concern that this method may induce artifactual negative correlations. To address this concern, we conducted additional analyses (*SI Materials and Methods, Functional Connectivity Analysis*) whereby we removed white matter and CSF confounds as an alternative to global signal regression (8). Results show that the majority of brain regions identified by using global signal regression (Fig. 2) were also identified after removing white matter and CSF confounds. Specifically, results show ASD underconnectivity in several structures of the reward circuit, including bilateral putamen, left-hemisphere NAc, dorsal caudate, anterior insula, and orbitofrontal cortex. Results also show ASD underconnectivity in visual processing regions, including right-hemisphere lateral occipital cortex, lingual gyrus, and fusiform gyrus. Consistent with results from global signal regression, no brain regions were identified for the ASD>TD contrast. Images are thresholded at $P < 0.01$ for voxel height and an extent of 100 voxels. FG, fusiform gyrus; LOC, lateral occipital cortex; OFC, orbitofrontal cortex.

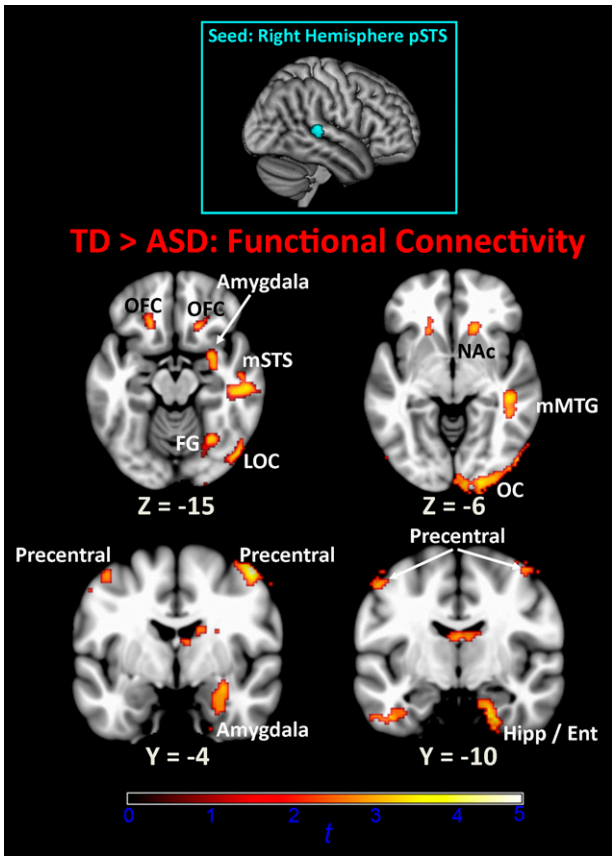

Fig. S7. Between-group functional connectivity results for right-hemisphere speech-selective cortex after removing white matter and CSF confounds. Similar to Fig. S6, we have conducted additional analyses (*SI Materials and Methods*, *Functional Connectivity Analysis*) whereby we removed white matter and CSF confounds as an alternative to global signal regression (8). Results show that the majority of brain regions identified by using global signal regression (Fig. 3) were also identified after removing white matter and CSF confounds. Specifically, results show ASD underconnectivity in right-hemisphere amygdala, mid-superior temporal gyrus, sulcus, and hippocampus, as well as bilateral orbitofrontal cortex and left-hemisphere NAc. Results also show ASD underconnectivity in visual processing regions, including right-hemisphere lateral occipital cortex, lingual gyrus, and fusiform gyrus, as well as bilateral precentral gyrus. Consistent with results from global signal regression, no brain regions were identified for the ASD>TD contrast. Images are thresholded at $P < 0.01$ for voxel height and an extent of 100 voxels. Ent, entorhinal cortex; FG, fusiform gyrus; Hipp, hippocampus; LOC, lateral occipital cortex; mMTG, mid-middle temporal gyrus; mSTS, mid-superior temporal sulcus; OC, occipital cortex; OFC, orbitofrontal cortex.

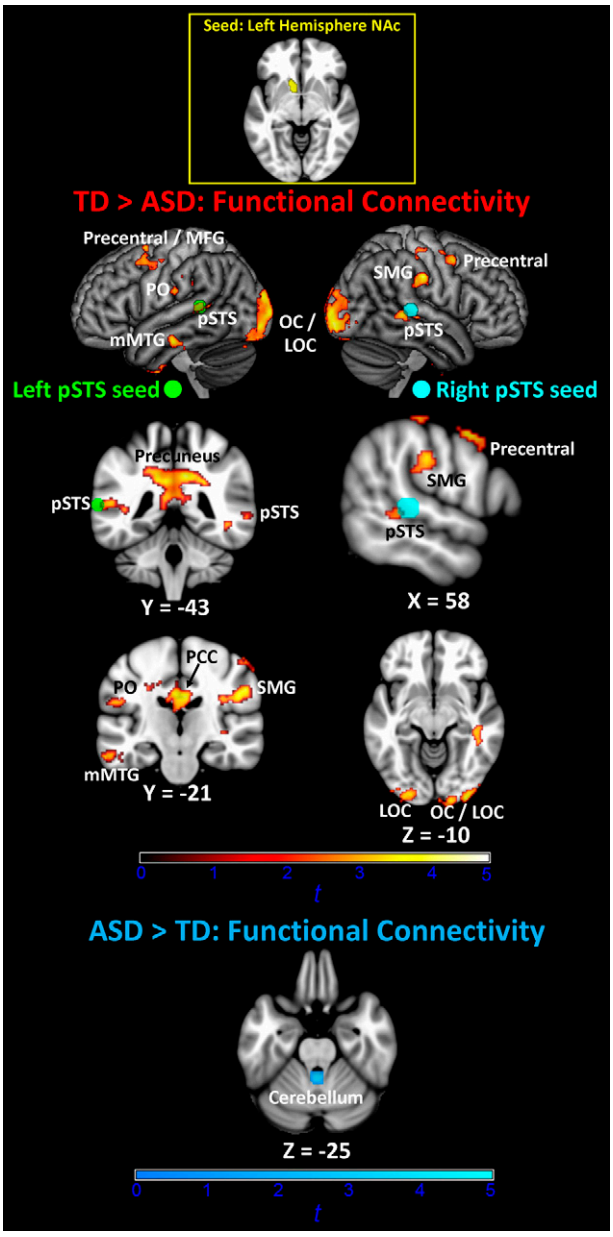

Fig. S8. Between-group functional connectivity results for left-hemisphere NAc. We performed this analysis to examine group differences in connectivity patterns originating from the reward circuit. Results show ASD underconnectivity between left-hemisphere NAc and several brain structures, including bilateral pSTS and left-hemisphere mMTG of temporal cortex, bilateral medial and lateral occipital cortex, bilateral precuneus, right-hemisphere supramarginal gyrus, left-hemisphere central operculum of parietal cortex, precentral gyrus, and posterior cingulate cortex. Only a small region of the anterior medial cerebellum showed ASD overconnectivity for the NAc seed (*Lower*). Images are thresholded at $P < 0.01$ for voxel height and an extent of 100 voxels. LOC, lateral occipital cortex; MFG, middle frontal gyrus; mMTG, mid-middle temporal gyrus; OC, occipital cortex; PCC, posterior cingulate cortex; PO, parietal operculum; SMG, supramarginal gyrus.

Table S1. Brain connections entered into brain-behavior regression analyses

Brain region	Coordinates
Left hemisphere pSTS	−63, −42, 9
Left hemisphere caudate	−18, 4, 20
Left hemisphere insula	−28, 18, −10
Left hemisphere NAc	−12, 18, −8
Left hemisphere putamen	−24, 14, −8
Left hemisphere OFC	−30, 24, −12
Right hemisphere pSTS	57, −31, 5
Right hemisphere VTA	2, −22, −20
Right hemisphere caudate	14, 22, −6
Right hemisphere NAc	14, 18, −8
Right hemisphere putamen	16, 14, −10
Right hemisphere amygdala	30, −4, −24

OFC, orbitofrontal cortex; VTA, ventral tegmental area.